CHEMISTRY OF MATERIALS
Cite This: Chem. Mater. 2019, 31, 6286−6294
Article
pubs.acs.org/cm

Data-Driven Discovery of Full-Visible-Spectrum Phosphor

Shuxing Li,[†] Yonghui Xia,[†] Mahdi Amachraa,[‡] Nguyen Tuan Hung,[§] Zhenbin Wang,*[,‡] Shyue Ping Ong,*[,‡] and Rong-Jun Xie*[,†]

[†]College of Materials, Xiamen University, Xiamen 361005, China
[‡]Department of Nanoengineering, University of California—San Diego, La Jolla, California 92093-0448, United States
[§]Frontier Research Institute for Interdisciplinary Sciences, Tohoku University, Sendai 980-8578, Japan

Supporting Information

ABSTRACT: The development of extra-broadband phosphors is essential for next-generation illumination with better color experience. In this work, we report the discovery of the first-known Eu^{2+}-activated full-visible-spectrum phosphor, $Sr_2AlSi_2O_6N:Eu^{2+}$, identified by combining data mining of high-throughput density functional theory calculations and experimental characterization. Excited by UV-light-emitting diodes (LEDs), $Sr_2AlSi_2O_6N:Eu^{2+}$ shows a superbroad emission with a bandwidth of 230 nm, the broadest emission bandwidth ever reported, and has excellent thermal quenching resistance (88% intensity at 150 °C). A prototype white LED utilizing only this full-visible-spectrum phosphor exhibits superior color quality (R_a = 97, R_9 = 91), outperforming commercial tricolor phosphor-converted LEDs. These findings not only show great promise of $Sr_2AlSi_2O_6N:Eu^{2+}$ as a single white emitter but also open up in silico design of full-visible-spectra phosphor in a single-phase material to address the reabsorption energy loss in commercial tricolor phosphor mixture.

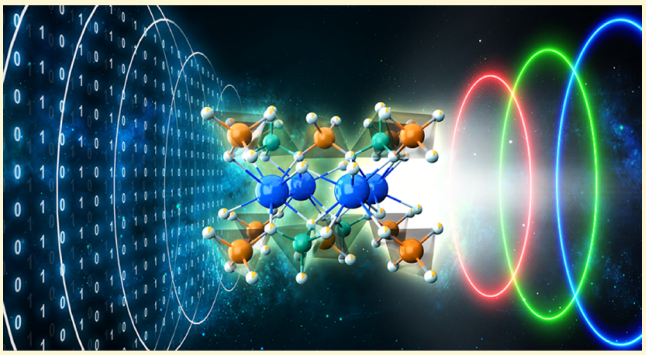

INTRODUCTION

Illumination sources based on phosphor-converted light-emitting diodes (pc-LEDs) are of great relevance to energy savings.[1−3] The typical commercial white LEDs based on blue LED chips and yellow-emitting phosphors suffer from "blue spike", "cyan gap", and deficiency of the red-light component, leading to severe problems of blue-light hazard, discomfort glare, and poor color rendition, respectively.[1,4,5] UV-pumped white LEDs utilizing UV-LED chips with a tricolor (blue/green/red) phosphor mixture have emerged as a promising alternative to improve the color quality of general illumination, valued by the Department of Energy solid-state lighting program.[6,7] Nevertheless, the tricolor phosphors have to be mixed homogeneously to avoid agglomeration, which in turn results in strong reabsorption energy loss (>20%) among the phosphor mixture and consequently decreases the efficiency of pc-LEDs. Moreover, it is challenging to control the color balance for phosphors mixture due to their different thermal quenching behaviors. The development of a single-phase broadband phosphor is therefore regarded as the best option to produce white light with high quality of illumination.

Recently, a few single-phase compounds have been reported as broadband white-emitting phosphors.[8−14] For example, Dai et al. reported the $Sr_5(PO_4)_{3-x}(BO_3)_xCl:0.04Eu^{2+}$ solid solution as a white-light phosphor by substituting PO_4 with BO_3 polyhedron in the $Sr_5(PO_4)_3Cl$ matrix.[8] This Eu^{2+}-activated solid solution showed an emission bandwidth (the full width at half-maximum or FWHM) of ∼137 nm but had severe thermal quenching (∼38% at 150 °C) and moisture sensitivity. Durach et al. later discovered $La_3BaSi_5N_9O_2:Ce^{3+}$ as a broadband (FWHM = ∼167 nm) yellow-emitting phosphor but did not evaluate its performance.[9] Zhu et al. investigated the luminescence properties of $Y_3Si_5N_9O:Ce^{3+}$, which exhibited an emission maximum at 620 nm and a broad bandwidth of 178 nm.[10] This phosphor has quite a large thermal quenching, and its emission intensity was reduced by 80% at 150 °C. The broadband emission of Ce^{3+}-activated phosphors could be attributed to the intrinsic large spin−orbital splitting (>2000 cm^{-1}) of the lowest 4f ($^2F_{5/2}$ and $^2F_{7/2}$) levels and multiple luminescent centers in the structure.[9,10,15] Despite extensive studies, no Eu^{2+}-activated single-phase compound has been discovered to be an extra-broadband (FWHM > 150 nm) white-emitting phosphor.

In principle, the (extra-) broadband emission of a Eu^{2+}-activated phosphor arises from its multiple luminescent centers, which could be achieved via two folds, (i) diverse local environments for Eu^{2+} and (ii) codoping Eu^{2+} with other activators (e.g., Eu^{3+} or Mn^{2+}) based on energy transfer.[11−14] The first approach offers a better manipulation of color stability, whereas the second one often suffers from poor color

Received: June 26, 2019
Revised: July 24, 2019
Published: August 2, 2019

DOI: 10.1021/acs.chemmater.9b02505
Chem. Mater. 2019, 31, 6286−6294

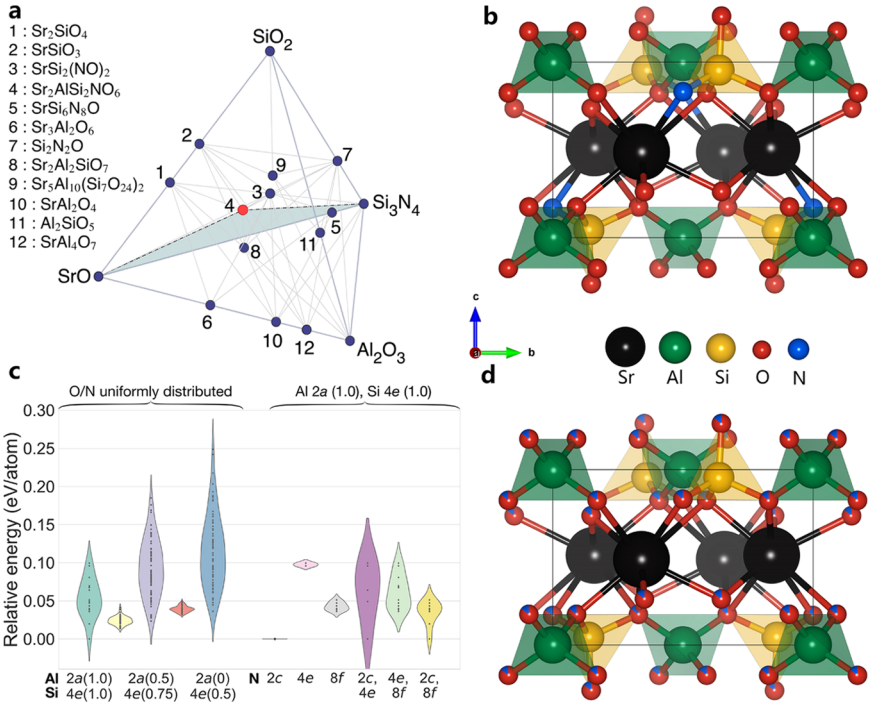

Figure 1. Computation-assisted discovery and structure analysis of $Sr_2AlSi_2O_6N$. (a) Calculated $SrO-SiO_2-Si_3N_4-Al_2O_3$ three-dimensional phase diagram at 0 K. Dark blue circles, known stable phases in the Materials Project database; red circle, new predicted phase, $Sr_2AlSi_2O_6N$. (b) Unit cell of the ordered $Sr_2AlSi_2O_6N$ structure. (c) Relative energies of distinct orderings of reconstructed $Sr_2AlSi_2O_6N$ structures. The left panel in (c) shows relative energy distributions of ordered configurations for structures with Al(2a)/Si(4e) occupancy changing from 1.0/1.0 to 0/0.5 and uniform O/N distributions. The occupancy change steps for Al(2a) and Si(4e) are 0.25 and 0.125, respectively. Only three Al/Si occupancies are labeled for the sake of brevity. The right panel shows relative energy distributions of ordered configurations for structures with N occupying a single 2c, 4e, 8f site or two of these three sites and Al(2a)/Si(4e) of 1.0/1.0. (d) Energetically favorable representation of the $Sr_2AlSi_2O_6N$ structure with Al(2a)/Si(4e) occupancy of 1.0/1.0 and uniformly disordered O/N.

stability because of distinct thermal quenching behaviors of different activators. The diverse local environments could be accessed using the host material with multiple nonequivalent doping sites or distinct ligands. Nowadays, new strategies, such as single-particle diagnosis,[16] mineral-inspired prototype evolution,[17] and combinatorial chemistry screening,[18] have been utilized in aiding new phosphors discovery. Among them, high-throughput first principles calculations have become a powerful tool by rapidly screening thousands of materials with properties of interest.[19−24] Very recently, an earth-abundant phosphor host Sr_2LiAlO_4 was discovered by high-throughput density functional theory (DFT) prediction and confirmed as a green/blue-emitting phosphor with Eu^{2+}/Ce^{3+} activation in the experiment, which is the first successful demonstration of in silico phosphor discovery for pc-LEDs.[21]

In this work, we report a full-visible-spectrum phosphor identified by combining density functional theory (DFT) prediction and experimental validation. We performed high-throughput screening for the selected Sr−Al−Si−O−N chemistry and propose structurally disordered $Sr_2AlSi_2O_6N$ as a promising host material for Eu^{2+}-activated broadband phosphors with good phase and thermal stabilities. The pure-phase $Sr_2AlSi_2O_6N:Eu^{2+}$ was successfully synthesized and measured to have an extra-broad emission bandwidth of 230 nm, which to the authors' knowledge is the broadest white-emitting phosphor in single-phase Eu^{2+} or Ce^{3+}-activated phosphors. Also, it has an excellent thermal quenching resistance, retaining 88% emission intensity at 150 °C. We also demonstrate that Sr site engineering via chemical substitution is a promising way to improve the quantum efficiency and the local structures of these substituted phosphors were elucidated using DFT calculations and Raman and NMR analyses. A prototype pc-LED utilizing the developed single-phase white-emitting phosphor yields white light with a correlated color temperature of 4000 K and high color rendering indexes (R_a = 97, R_9 = 91).

RESULTS AND DISCUSSION

Host Material Identification. As previous studies have shown, the presence of multiple activator local environments can result in emission spectra broadening in phosphors.[25,26] In this work, our focus is on new phosphor discovery in the relatively unexplored Sr−Al−Si−O−N quintenary chemistry. This choice is guided by the hypothesis that the relatively similar ionic radii of the cations Al^{3+} and Si^{4+} as well as the anions N^{3-} and O^{2-} provide an immense scope for the formation of compositionally tunable disordered solid solution phases, for example, as seen in the SiAlON family of compounds.[3,27] The high-throughput framework[21,28] used in this work is depicted in Figure S1. By applying a data-mined ionic substitution algorithm on all prototype structures in ICSD-2017, a total of 496 novel candidate phosphor hosts in the Sr−Al−Si−O−N chemical space were generated (see the Supporting Information worksheet). The first criterion that any technological material must satisfy is the phase stability. We constructed the 0 K DFT phase diagram based on known stable phases available in Materials Project[29] for Sr−Al−Si−O−N chemistries and then computed the energy above the linear combination of stable phases in this phase diagram, also known as E_{hull}, to estimate the thermodynamic stability of a

DOI: 10.1021/acs.chemmater.9b02505
Chem. Mater. 2019, 31, 6286−6294

predicted compound. Similar to previous DFT HT screening works,[28,30] we adopted a conservative E_{hull} threshold of 50 meV/atom to pinpoint thermodynamically stable or metastable phases. As a phosphor host, the compound is expected to have an appropriate host band gap for visible emission when activated with Eu^{2+}/Ce^{3+}. Our previous work found that there is an inverse relationship between experimental wavelength and the DFT computed host band gap (E_g) using the Perdew–Burke–Ernzerhof (PBE) functional.[28,31] We therefore limited the PBE E_g ranging from 3.0 to 5.5 eV for visible emission. A phosphor with a large host band gap and rigid structure also tends to be thermal stable due to the large photoionization energy.[32,33] We then used the more accurate Heyd–Scuseria–Ernzerhof (HSE) functional[34,35] to predict the host band gap. The structure rigidity was estimated by the DFT-calculated Debye temperature (Θ_D). Table S1 summarizes the predicted three promising phosphor hosts, among which $Sr_2AlSi_2O_6N$ is emerged as the most promising candidate in terms of phase stability, large host band gap, and high Debye temperature. The other two materials, $Sr_3AlSi_3O_9N$ and $SrAl_2Si_3O_4N_4$, are predicted to be metastable, signifying that more efforts might be devoted to their synthesis.

The crystal structure of $Sr_2AlSi_2O_6N$ (space group: $P\bar{4}2_1m$) is derived from $Ba_2ZnGe_2S_6O$ (ICSD no. 14174) via a multispecies substitution of Ba^{2+} with Sr^{2+}, Zn^{2+} with Al^{3+}, Ge^{4+} with Si^{4+}, S^{2-} with O^{2-}, and O^{2-} with N^{3-}. $Sr_2AlSi_2O_6N$ exhibits alternating Sr and Si/Al layers with a single Sr crystallographic site, shown in Figure 1b. DFT computations predict that $Sr_2AlSi_2O_6N$ is thermodynamically (E_{hull} = 0, see Figure 1a)[29] and dynamically (see Figure S2) stable, with PBE and HSE host band gaps (E_g) of 3.82 and 5.41 eV, respectively, and a rigid crystal structure (Θ_D = 525 K). According to the reported inverse relationship between experimental wavelength and the PBE E_g,[28] $Sr_2AlSi_2O_6N$ is predicted to yield orange-red emission when activated by Eu^{2+}.

Given the high-temperature synthesis conditions for oxynitrides and the relatively similar ionic radii of Al^{3+}/Si^{4+} and O^{2-}/N^{3-}, we performed further investigations of Al/Si and O/N disorder on the stability of $Sr_2AlSi_2O_6N$. Based on the fully disordered $Sr_2AlSi_2O_6N$ structure, Al and Si can occupy the 2a and 4e sites, while O and N occupy the 2c, 4e, and 8f sites. To keep the number of computations tractable, cation and anion disorders are modeled independently using an approximate mean-field approach. First, different Al/Si occupancies are assigned to the 2a and 4e sites such that the overall composition is that of stoichiometric $Sr_2AlSi_2O_6N$, while a uniform anion occupancy is assigned to the 2c, 4e, and 8f sites. It is found that the lowest energy cation ordering is one where Al fully occupies the 2a site and Si fully occupies the 4e site. This occupancy preference is also confirmed by our Raman and solid-state nuclear magnetic resonance (NMR) results (vide infra). The site occupancies explored are summarized in Table S2. The corresponding crystal structures are illustrated in Figure S3. The relative energies of distinct orderings of refined $Sr_2AlSi_2O_6N$ structures are sorted in Figure 1c. Based on the preferred cation ordering, we explored different anion occupancies. We find that while full N occupancy on the 4e sites is clearly unfavorable, partial occupancy of N on 2c, 4e, and 8f results in structures that are relatively close in energy (<50 meV/atom difference). Considering the high sintering temperature of $Sr_2AlSi_2O_6N$, we have constructed the anion-disordered structure model given in Figure 1d with Al (2a), 1.0; Si (4e), 1.0; and uniformly disordered N/O.

Synthesis of the Predicted Compound. The predicted $Sr_2AlSi_2NO_6$ was successfully synthesized using the solid-state reaction. Figure 2 shows the simulated and experimental X-ray

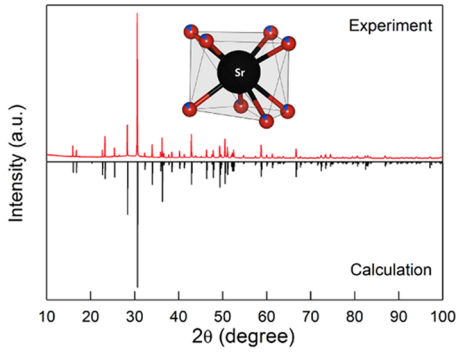

Figure 2. Measured (red) and calculated (black) X-ray powder diffraction patterns of $Sr_2AlSi_2O_6N$. The inset is the square antiprism $Sr(O/N)_8$ polyhedron.

diffraction (XRD) profiles of $Sr_2AlSi_2O_6N$, which are in excellent agreement with each other, confirming the successful synthesis of the predicted $Sr_2AlSi_2O_6N$ compound. The predicted crystal structure (Figure 1d) of $Sr_2AlSi_2O_6N$ was used for the XRD Rietveld analysis and the residual factors are R_{wp} = 6.10% and R_p = 4.67% (Figure S4). The inset presents the square antiprism $Sr(O/N)_8$ polyhedron. The disordering of Al/Si and O/N atoms in $Sr_2AlSi_2O_6N$ unambiguously indicates distinct local environments for Eu^{2+}, which are of great benefit to broadband emission.

Photoluminescence (PL) Properties. The 1 mol % Eu^{2+} concentration for $Sr_{2-y}AlSi_2O_6N:yEu^{2+}$ was optimized in terms of its quantum yield (QY) and absorption efficiency (Figure S5) and then used for photoluminescence properties investigations. Figure 3a,b presents the measured photoluminescence spectra of $Sr_2AlSi_2O_6N:Eu^{2+}$. The excitation spectrum shows a strong absorption centered at 330 nm ranging from 250 to 450 nm. Under the excitation of 330 nm, a bright white emission light is achieved. The emission spectrum has an unprecedented broadband spanning from 400 to 850 nm with a bandwidth of 230 nm, covering the full visible spectrum and peaking at 600 nm. Since there is only one crystallographic site for Eu^{2+} activation, the broad emission is attributed to the multiple local environments for Eu^{2+} activators introduced by the disordering of both Al/Si and O/N. To further confirm the multiple luminescent centers, we collected the decay curve monitored at 600 nm under the excitation of 330 nm, as plotted in Figure 3c. The decay curve can be well fitted into the following double-exponential function[36]

$$I = A_1 \exp\left(-\frac{t}{\tau_1}\right) + A_2 \exp\left(-\frac{t}{\tau_2}\right)$$

According to the fitted values of τ_1 (160.5 ns), τ_2 (1304.6 ns), and their percentage contents, the average lifetime calculated is 1.14 μs. The τ_2 value is in line with the typical radiative decay of Eu^{2+}, whereas the smaller τ_1 value implies a fast decay behavior, which is possibly related to the energy transfer process between Eu^{2+} activators in different local environments. The low-temperature (10 K) decay curves (see Figure S6) of $Sr_2AlSi_2O_6N:Eu^{2+}$ recorded with respect to the detection wavelength from 400 to 800 nm show that the

DOI: 10.1021/acs.chemmater.9b02505
Chem. Mater. 2019, 31, 6286–6294

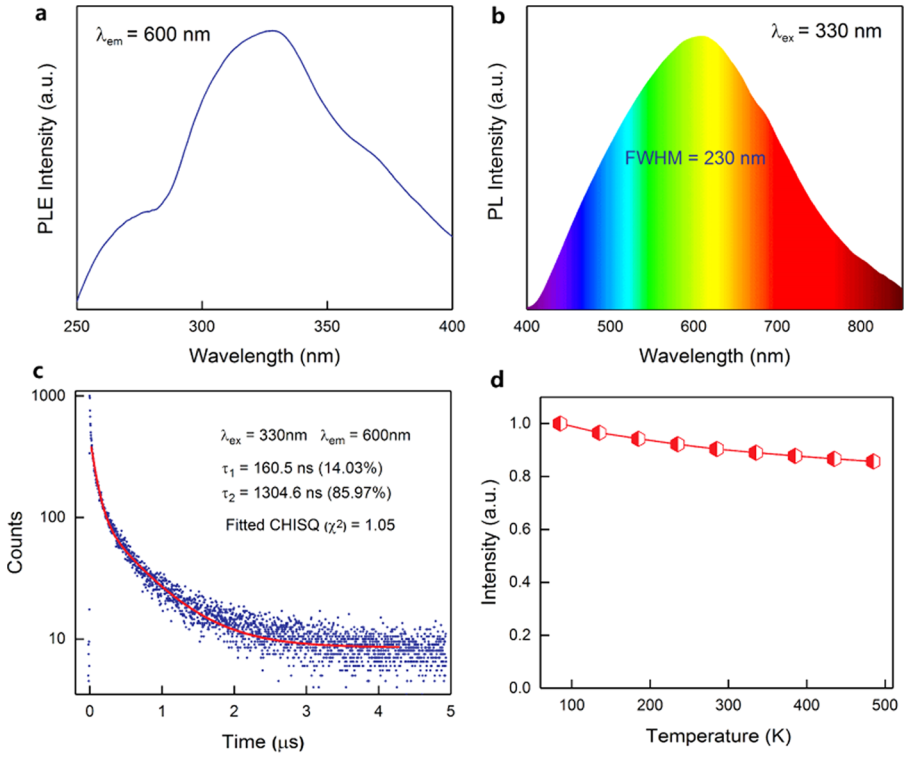

Figure 3. Photoluminescence properties of white-emitting $Sr_2AlSi_2O_6N:Eu^{2+}$. (a) Excitation and (b) emission spectra measured at room temperature. (c) Luminescent decay curves of $Sr_2AlSi_2O_6N:Eu^{2+}$ monitored at 600 nm under the excitation of 330 nm. (d) Temperature dependence of the peak emission intensity.

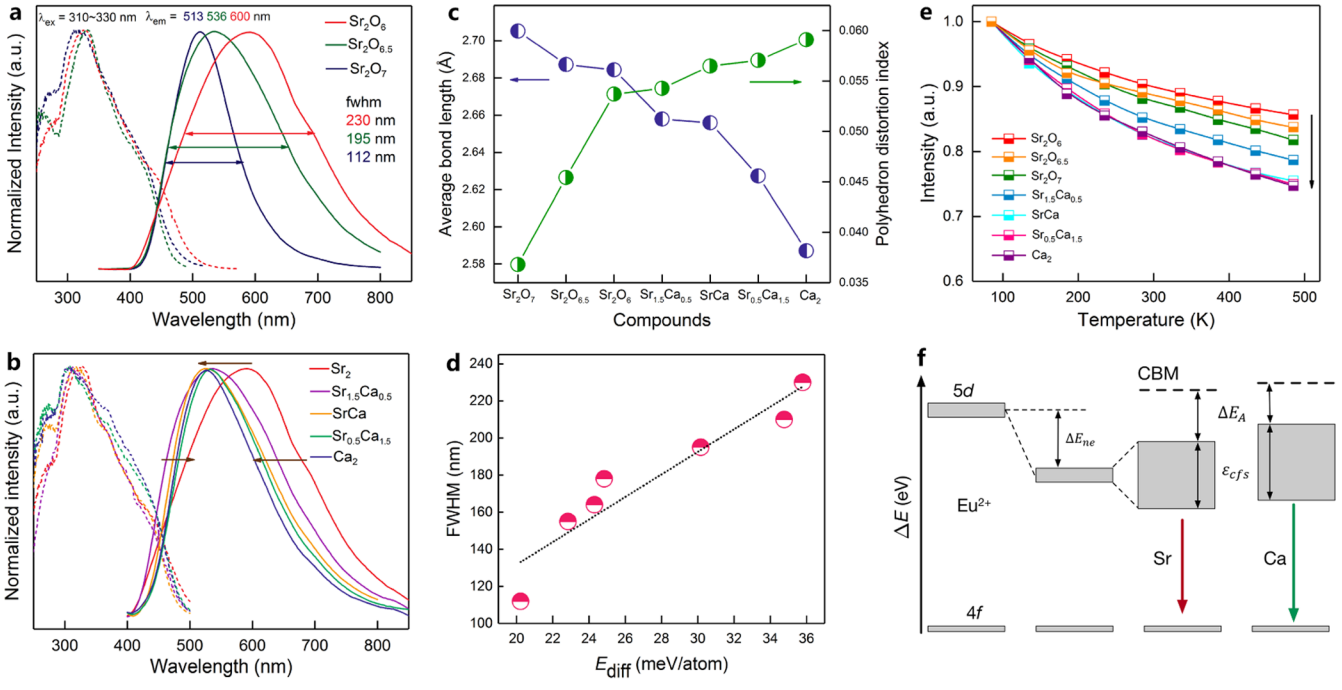

Figure 4. Photoluminescence evolutions of $Sr_2AlSi_2O_6N:Eu^{2+}$-based compounds by chemical substitutions. Excitation and emission spectra of (a) $Sr_2Al_{1+x}Si_{2-x}O_{6+x}N_{1-x}:Eu^{2+}$ (x = 0−1) and (b) $Sr_{2-z}Ca_zAlSi_2O_6N:Eu^{2+}$ (z = 0−2) under the excitation of 310−330 nm ($Sr_2Al_2SiO_7$ (Sr_2O_7), $Sr_2Al_{1.5}Si_{1.5}O_{6.5}N_{0.5}$ ($Sr_2O_{6.5}$), $Sr_2AlSi_2O_6N$ (Sr_2O_6), $Sr_{1.5}Ca_{0.5}AlSi_2O_6N$ ($Sr_{1.5}Ca_{0.5}$), $SrCaAlSi_2O_6N$ (SrCa), $Sr_{0.5}Ca_{1.5}AlSi_2O_6N$ ($Sr_{0.5}Ca_{1.5}$), and $Ca_2AlSi_2O_6N$ (Ca_2)). (c) Average bond length (d_{av}) and polyhedron distortion index (D) results from Rietveld refinements. (d) Relationship between site energy difference (E_{diff}) and FWHM. (e) Thermal quenching behaviors of $Sr_2AlSi_2O_6N:Eu^{2+}$-based phosphors. (f) Schematic energy-level diagram for Eu^{2+} in $Sr_2AlSi_2O_6N$ and $Ca_2AlSi_2O_6N$ host structures.

luminescence decays faster at a shorter wavelength than that at a longer wavelength, which is a typical behavior of energy transfer.[37,38] The QY of broadband phosphors tends to be inherently lower than narrow-band phosphors. Nevertheless, it

DOI: 10.1021/acs.chemmater.9b02505
Chem. Mater. 2019, 31, 6286−6294

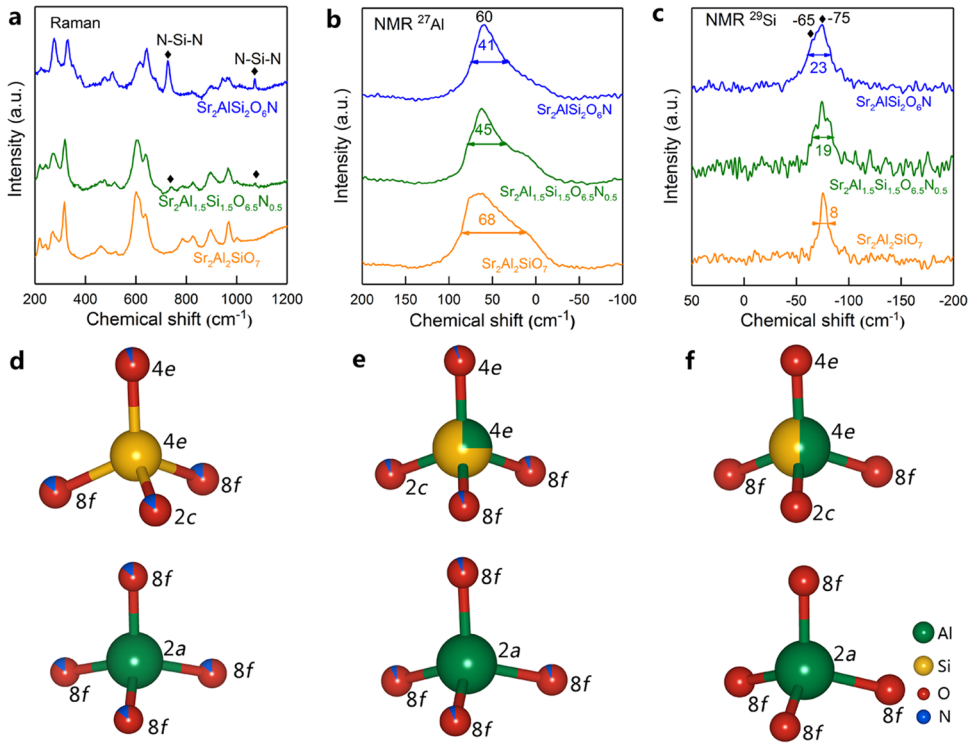

Figure 5. Local structure analysis of $Sr_2Al_{1+x}Si_{2-x}O_{6+x}N_{1-x}:Eu^{2+}$ ($x = 0-1$) compounds. (a) Raman spectra. (b) Solid-state ^{27}Al MAS NMR spectra. (c) Solid-state ^{29}Si MAS NMR spectra. Local coordination environments of $Si(O/N)_4$ and $Al(O/N)_4$ for (d) $Sr_2AlSi_2O_6N$, (e) $Sr_2Al_{1.5}Si_{1.5}O_{6.5}N_{0.5}$, and (f) $Sr_2Al_2SiO_7$.

is compensated by the fact that the extra-broadband phosphor avoids the reabsorption energy loss (>20%) that tricolor phosphor mixture severely suffers from because of large spectral overlapping.

For practical applications, thermal stability is another critical parameter for phosphor materials. As shown in Figure 3d, the temperature-dependent emission intensity measured from 80 to 500 K reveals that $Sr_2AlSi_2O_6N:Eu^{2+}$ possesses an excellent thermal quenching resistance. The emission intensity maintains 88% at 423 K (150 °C) with respect to 80 K. We then collected the temperature-dependent lifetime curves as a function of temperature from 10 to 500 K (Figure S7). The change in the lifetime is consistent with that of the luminescent intensity, reconfirming the excellent thermal quenching resistance of $Sr_2AlSi_2O_6N:Eu^{2+}$. These findings show great promise of $Sr_2AlSi_2O_6N:Eu^{2+}$ as a single white-emitting phosphor for high-quality white LEDs.

Chemical Substitutions. To further improve the quantum efficiency of this highly promising full-visible-spectrum phosphor, we explored various chemical substitutions. Taking $Sr_2AlSi_2O_6N$ as the parent structure, we generated seven new compositions by substituting Al−O ↔ Si−N or Sr → Ca/Ba and then evaluated their structural and electronic properties relating to photoluminescence using DFT calculations. The calculated results are summarized in Table S3. Three of them are particular promising because of their good phase stability ($E_{hull} = 0$). $Sr_2Al_2SiO_7:Eu^{2+}$ has already been reported as a cyan-emitting phosphor,[39] which confirms the reliability of our approach in search of new phosphors. It should be noted, however, that while there have been many previous attempts at Al−O ↔ Si−N substitution in $Sr_2Al_2SiO_7$, none has succeeded in achieving a N doping concentration of more than 0.6.[40] We then synthesized seven phosphors with compositions of $Sr_2Al_{1+x}Si_{2-x}O_{6+x}N_{1-x}:Eu^{2+}$ ($x = 0-1$) and $Sr_{2-z}Ca_zAlSi_2O_6N:Eu^{2+}$ ($z = 0-2$). These compounds maintain high phase purity across the entire substitution range examined, as described in Figures S8 and S9. The primary peak in the XRD profiles of $Sr_2Al_{1+x}Si_{2-x}O_{6+x}N_{1-x}:Eu^{2+}$ ($x = 0-1$) shifts toward lower angles with increasing x, whereas the one in $Sr_{2-z}Ca_zAlSi_2O_6N:Eu^{2+}$ ($z = 0-2$) moves to higher angles with increasing z. The former can be ascribed to the replacement of Si−N bonds by the slightly longer Al−O bonds, and the latter is due to the substitution of smaller Ca atoms for Sr atoms. These changes are also confirmed by the fitted lattice parameters from X-ray Rietveld refinement analysis (Table S4).

Next, we carried out a comprehensive investigation on the relationship between compositions and photoluminescence properties. With increasing x in $Sr_2Al_{1+x}Si_{2-x}O_{6+x}N_{1-x}:Eu^{2+}$ ($x = 0-1$), the emission peak is blue-shifted from 600 to 513 nm and the corresponding bandwidth decreases from 230 to 112 nm (Figure 4a). A similar blue shift in emission peaks (600 → 525 nm) and a decrease of bandwidth (230 → 155 nm) are also observed for $Sr_{2-z}Ca_zAlSi_2O_6N:Eu^{2+}$ ($z = 0-2$) with increasing z, as displayed in Figure 4b. It is generally accepted that the shift of emission maximum can be attributed to the centroid shift of Eu free ion and crystal field splitting (CFS) of the Eu 5d orbitals.[1,3,41] Smaller centroid shift and weaker crystal field splitting lead to a blue shift in emission. The centroid shift is related to the nephelauxetic effect. The higher the Eu−O/N bond covalency, the larger the centroid shift. The magnitude of CFS is determined by the Eu−O/N local geometry, which can be described by the average bond length (d_{av}) and distortion index (D) of the square antiprism $Eu(O/N)_8$ polyhedron in terms of $D = \frac{1}{n}\sum_{i=1}^{n}\frac{|d_i - d_{av}|}{d_{av}}$. A shorter

DOI: 10.1021/acs.chemmater.9b02505
Chem. Mater. 2019, 31, 6286−6294

bond length and a higher distortion index typically result in a larger CFS. Given the stronger covalency of Sr−N bonds than Sr−O ones, the centroid shift decreases with increasing x in $Sr_2Al_{1+x}Si_{2-x}O_{6+x}N_{1-x}:Eu^{2+}$ (x = 0−1). Meanwhile, based on the XRD Rietveld refinement analysis (Figure 4c), the average Eu−O/N bond length expands, while the distortion index decreases with increasing x in $Sr_2Al_{1+x}Si_{2-x}O_{6+x}N_{1-x}:Eu^{2+}$ (x = 0−1), both of which signify a weaker CFS and consequently lead to a blue shift in emission. Similarly, with increasing z in $Sr_{2-z}Ca_zAlSi_2O_6N:Eu^{2+}$ (z = 0−2), the centroid shift is expected to be untouched considering their same Eu−O/N local environments and the Eu−O/N bond length and Eu(O/N)$_8$ polyhedron are seen to become shorter and more distorted, respectively. This interpretation implies that Eu atoms experience a stronger CFS, which will result in a red shift, contradicting our experimental findings. We argue that the enlarged host band gap (see Table S3) is responsible for this blue shift, which is also observed in β-SiAlON:Eu^{2+}.[42] Although the emission bandwidths decrease significantly, their emission spectra are still broader than the general Eu^{2+} emissions (FWHM = 90−120 nm).[26] To shed light on the changes of emission bandwidth, we calculated the Eu site energy difference (E_{diff}) between the most energetically favorable and unfavorable ordered structures for each phosphor using DFT calculations. We find that there is a positive relationship between the Eu site energy difference and measured emission bandwidth (Figure 4d). The larger the E_{diff}, the further the two end luminescent centers, signifying a broader emission spectrum. We also observe a big jump in emission bandwidth from $Sr_2Al_{1.5}Si_{1.5}O_{6.5}N_{0.5}$ to $Sr_2Al_2SiO_7$ (195 → 112 nm), which unambiguously proves the critical role of structural disorder in the broadband emission.

Figure 4e presents the measured thermal stability of these substituted phosphors. After chemical substitutions, the phosphors show some decrease in thermal stability but still possess good thermal quenching resistance by maintaining >77% of the initial intensity at 423 K (150 °C). The slightly decreased thermal stability is due to the upward shifting of excited Eu 5d orbitals accompanied with the blue-shift emission (Figure 4f). As shown in Table S5, the QYs of $Sr_{2-z}Ca_zAlSi_2O_6N:Eu^{2+}$ (z = 0−2) phosphors increase by a factor of 2 from 7.9 to 19.1%. These findings suggest that engineering Sr sites by partial substitutions is a promising way to further optimize its performance in future works.

Structure Evolution. The Al−O chemical substitution renders the structure of $Sr_2AlSi_2O_6N$ more complex, and here, we take advantage of Raman spectra and solid-state nuclear magnetic resonance (NMR) to provide direct insights into the local structure. Figure 5a shows the measured Raman spectra of $Sr_2Al_{1+x}Si_{2-x}O_{6+x}N_{1-x}:Eu^{2+}$ (x = 0−1) with sharp vibrational peaks ranging from 200 to 1200 cm^{-1}. We note that the two peaks at around 730 and 1070 cm^{-1}, identified to be the stretching vibrations of N−Si−N bond based on the density functional perturbation theory (DFPT) calculations, fade away with increasing x. This indicates that Si has a preference to reside at the 4e Al/Si site, bonding one 2c O/N, one 4e O/N, and two 8f O/N, not at the 2a Al/Si site where it is coordinated to four identical 8f O/N. The peak with relatively higher Raman intensity at 730 cm^{-1} can be attributed to the vibrations of doublet N(2c)−Si(4e)−N(8f) and the other one is likely due to the vibration of singlet N(8f)−Si−N(8f) since N is energetically unfavorable to locate at 4e O/N site based on our previous DFT results. These observations verify our DFT predictions of Al/Si and O/N sites occupying tendency (see Figure 1c).

Figure 5b,c presents the ^{27}Al and ^{29}Si solid-state NMR spectra of $Sr_2Al_{1+x}Si_{2-x}O_{6+x}N_{1-x}:Eu^{2+}$ (x = 0−1), respectively. The chemical shifts of ^{27}Al at 60 ppm and ^{29}Si at −75 ppm arise from [AlO_4] and [SiO_4] tetrahedral units, respectively.[43,44] With increasing x, the resonance bandwidth in NMR ^{27}Al spectra broadens from 41 to 68 ppm and it narrows down from 23 to 8 ppm in NMR ^{29}Si spectra. This is likely because at higher x, Al atoms not only fully occupy 2a Al/Si but also partially take up 4e Al/Si sites (Figure 5d−f). In particular, the shoulder at −65 ppm in NMR ^{29}Si spectra is assigned to the [SiO_2N_2] tetrahedron.[45] It can be clearly seen that the intensity of this shoulder gradually decreases with increasing x. This observation is consistent with our Raman spectra results for N−Si−N bonds and consequently reconfirms the critical role of the structure disorder in broadband emission.

Finally, this novel broadband white-emitting phosphor was evaluated for practical applications. By employing $Sr_2AlSi_2O_6N:Eu^{2+}$ as a single emitter, we fabricated a prototype white LED. The Commission Internationale de l'Eclairage (CIE) 1931 color coordinates are located right near the Blackbody with very small chromaticity drift when the forward bias driving current increases from 100 to 350 mA, as summarized in Table S6. The chromaticity shift (ΔE) is calculated to be as small as 7.7×10^{-3} using the following equation

$$\Delta E = \sqrt{(u'_f - u'_i)^2 + (v'_f - v'_i)^2 + (w'_f - w'_i)^2} \quad (1)$$

where $u' = 4x/(3 - 2x + 12y)$, $v' = 9y/(3 - 2x + 12y)$, and $w' = 1 - v' - u'$. u' and v' are chromaticity coordinates in the $u'v'$ uniform color space. x and y are chromaticity coordinates in CIE1931 color space, and i and f represent 100 and 350 mA, respectively. Given stable driving current of 300−350 mA, excellent color quality was obtained with R_a = 97 and R_9 = 91. The corresponding spectrum and photograph are displayed in Figure S10. The full-visible-spectrum emission of this single-phase phosphor makes the white light color quality even outperform that of tri-phosphor-converted white LEDs.[46] These results demonstrate that this newly discovered phosphor has great potential to serve as white-emitting phosphor for high-color-quality lighting applications.

CONCLUSIONS

In summary, leveraging on DFT structure prediction and photoluminescence (PL)-related properties calculation, we have discovered a novel $Sr_2AlSi_2O_6N$ phosphor host with good phase and thermal stability. Our DFT calculations further show that the $Sr_2AlSi_2O_6N$ structure is highly disordered and flexible, which is of great benefit to broadband emissions. The PL measurements indicate that $Sr_2AlSi_2O_6N:Eu^{2+}$ has a full-visible-spectrum emission with a minimal thermal quenching up to 500 K. We have also evidenced that the chemical substitution, particularly, by engineering the Sr sites, is a promising route to optimize the PL properties. The Raman and NMR spectra analyses uncover the structure evolutions introduced by the chemical substitutions and confirm the DFT structure prediction of Al/Si and O/N sites occupying tendency. The white LED fabricated using the as-discovered single-phase full-visible-spectrum phosphor shows excellent color quality (R_a = 97, R_9 = 91), superior to some tricolor pc-

DOI: 10.1021/acs.chemmater.9b02505
Chem. Mater. 2019, 31, 6286−6294

LEDs. The strategy reported in this work provides a general pathway to the discovery of single-phase full-visible-spectrum phosphor for white LEDs with superior color quality.

MATERIALS AND METHODS

Computational Methods. All density functional theory (DFT) calculations were performed using the Vienna ab initio simulation package within the projector-augmented wave method.[47,48] We used the generalized gradient approximation Perdew–Burke–Ernzerhof (PBE) functional for structure relaxation and energy calculations.[30] The plane wave energy cutoff was 520 eV, and the Brillouin zones were integrated with a k-point density grid at least 100/Å^{-3} (reciprocal lattice volume). All properties calculations for host materials unless stated otherwise were carried out with parameters in line with the Materials Project.[29] All crystal structure manipulations and data analysis were performed using the Python Materials Genomics (Pymatgen) package.[49]

The dynamic stability of host materials was evaluated by computing the phonon spectrum using the finite difference method implemented in the Phonopy code.[50] The energy and force criteria of 1e^{-8} eV and 1e^{-4} eV/Å, respectively, were used for these calculations. The host band gap was evaluated using both Perdew–Burke–Ernzerhof (PBE) functional and hybrid functional Heyd–Scuseria–Ernzerhof (HSE).[34,35] The Debye temperature (Θ_D) was calculated using the quasi-harmonic model.[33] The elastic tensor was calculated with an electronic energy convergence criterion of 10^{-6} eV, and the elastic moduli were then calculated using the Voigt–Reuss–Hill approximation. The nonresonant Raman spectra is obtained from the density functional perturbation theory (DFPT) calculations by the Quantum Espresso package.[51] We use a local-density approximations with norm-conserving pseudopotential.[52] The kinetic energy cutoff for wave functions was set at 120 Ry. The Monkhorst–Pack scheme with 2 × 2 × 4 mesh was used to sample k-points of the Brillouin zone.

For calculations of Eu^{2+}-activated phosphors, we used the PBE + U method with a Hubbard U value of 2.5 eV for Eu.[53,54] Supercell models of 2 × 2 × 2 were adopted to simulate the low Eu concentration in the experiment. The structures of these models were fully relaxed with energies and forces converged to within 10^{-5} eV and 0.01 eV/Å, respectively.

The initial candidates for the Sr–Al–Si–O–N chemistry were generated by applying the data-mined ionic substitution algorithm on the prototype structures in the 2017 version of ICSD.[55,56] This algorithm proposed a mathematically framework to evaluate the substitution probability of one species for another one with the same crystal structure.

Sample Preparation. The phosphor powders of $Sr_2Al_{1+x}Si_{2-x}O_{6+x}N_{1-x}:Eu^{2+}$ (x = 0–1), $Sr_{2-y}AlSi_2O_6N:yEu^{2+}$ (y = 0.002–0.06), and $Sr_{2-z}Ca_zAlSi_2O_6N:Eu^{2+}$ (z = 0–2) were prepared via a two-step synthesis method. Commercially available starting materials, such as $SrCO_3$, $CaCO_3$, Eu_2O_3, Si_3N_4, SiO_2, and Al_2O_3, were mixed homogeneously according to the target chemical compositions. The mixtures were loaded into the BN crucibles and fired in a horizontal tube furnace at 1380 °C for 4 h under a N_2–10% H_2 atmosphere. The as-prepared powders were pulverized by hand and subsequently fired in a gas pressure sintering furnace (Shimadzu, Kyoto, Japan) at 1400 °C for 4 h under a nitrogen pressure of 0.9 MPa. Finally, the fired samples were finely ground for further characterization.

Sample Characterizations. The crystal structure was determined by the X-ray diffraction (XRD) patterns collected with a powder X-ray diffractometer (D8 Advance, Bruker, Germany) with Cu Kα radiation at 40 kV and 40 mA. The Rietveld refinement was carried out by the General Structure Analysis System package within the EXPUGUI interface.[57] The photoluminescence (PL) spectra were measured with a steady-state fluorescence spectrometer (FLS980, Edinburgh Instruments Ltd., U.K.) equipped with a 450 W Xe lamp. The PL decay curves were collected using an FLS980 spectrometer with an nF920 nanosecond flashlamp. Pure hydrogen was used as the nF920 filler gas to produce a broad spectral continuum as the excitation source. The excitation wavelength was selected as the relative maxima (310–330 nm) in excitation intensity for each sample. The quantum efficiency was measured with an absolute PL quantum yield spectrometer (Quantaurus-QY, Hamamatsu Photonics, Tokyo, Japan) under the excitation of the relative maxima (310–330 nm) in excitation intensity for each sample. The thermal quenching behavior was tested using a steady-state fluorescence spectrometer (FLS980, Edinburgh Instruments Ltd., U.K.) equipped with a temperature controller (Model 336, Lake Shore Cryotronics) in a range from 85 to 485 K with a step of 50 K and a heating rate of 100 K/min. The excitation wavelength was set at the relative maxima in excitation intensity for each sample (310–330 nm). The solid-state ^{29}Si and ^{27}Al NMR experiments were performed at room temperature on a NMR 400 MHz spectrometer (Bruker AVANCE III, Switzerland). A Bruker 4 mm H–X magic-angle spinning (MAS) probe head was used with a MAS rate of 12 kHz. Raman spectra were performed using a solid-state laser excitation (785 nm) with a source power of 50 mW and resolution of 3 cm^{-1} (model XploRA, Horiba J. Y., France). The prototype warm white LEDs were fabricated using a Chip-on-Board packaging solution by pumping the $Sr_2AlSi_2O_6N:Eu^{2+}$ white-emitting phosphor using a high-power UV LED of 4 W (λ_{em} = 375–380 nm, Shenzhen Chundaxin Photoelectric Co., Ltd., Shenzhen, China). The optical properties of these white LEDs were recorded using an autotemperatured LED otpo-electronic analyzer (ATA-500, Everfine Co., Hangzhou, China). The white LED was driven under a bias current from 100 to 350 mA.

ASSOCIATED CONTENT

Supporting Information

The Supporting Information is available free of charge on the ACS Publications website at DOI: 10.1021/acs.chemmater.9b02505.

High-throughput screening workflow, calculated phonon spectrum, $Sr_2AlSi_2O_6N$ structures with different site occupancies, Rietveld refinement, quantum yields as a function of Eu concentration, low-temperature (10 K) decay curves, temperature-dependent (10–500 K) decay curves, XRD patterns of new compounds by chemical substitutions, as-fabricated white LED (PDF)

Generated 496 novel candidates in the Sr–Al–Si–O–N chemical space (XLSX)

AUTHOR INFORMATION

Corresponding Authors

*E-mail: z9wang@eng.ucsd.edu (Z.W.).
*E-mail: ongsp@eng.ucsd.edu (S.P.O.).
*E-mail: rjxie@xmu.edu.cn (R.-J.X.).

ORCID

Shuxing Li: 0000-0001-8086-7154
Nguyen Tuan Hung: 0000-0003-4156-6230
Zhenbin Wang: 0000-0002-7016-9245
Shyue Ping Ong: 0000-0001-5726-2587
Rong-Jun Xie: 0000-0002-8387-1316

Author Contributions

S.P.O. and R.-J.X. supervised the project. Z.W., S.P.O., and R.-J.X. designed the study. Z.W. performed the DFT calculations, analyzed the data, and prepared the manuscript. S.L. conducted the experiments, analyzed the data, and prepared the initial draft of the manuscript. Y.X. helped with the optical measurements. M.A. helped with thermal quenching analysis. N.T.H. conducted the density functional perturbation theory (DFPT) calculations to identify the Raman spectra. All authors contributed to the discussions and revisions of the manuscript.

DOI: 10.1021/acs.chemmater.9b02505
Chem. Mater. 2019, 31, 6286–6294

Notes

The authors declare no competing financial interest.

■ ACKNOWLEDGMENTS

The authors are grateful to the financial supports from the National Natural Science Foundation of China (Nos. 51832005, 51802274, 5157223, and 51561135015), National Key Research and Development Program (MOST, 2017YFB0404301), National Postdoctoral Program for Innovative Talents (No. BX201700138), and China Postdoctoral Science Foundation Grant (No. 2017M622073). The computational work was supported by the National Science Foundation, Ceramics Program, under Grant No. 1411192. The computational resources were provided by the Triton Shared Computing Cluster (TSCC) at the University of California, San Diego, the National Energy Research Scientific Computing Center (NERSC), and the Extreme Science and Engineering Discovery Environment (XSEDE) supported by the National Science Foundation under Grant No. ACI-1053575. Yuwei Yu and Zhuobin Xu from Information and Network Center of Xiamen University are acknowledged for help with high-performance computing. The authors also show sincere thanks to Peng Zheng for the fabrication and measurements of white LEDs.

■ REFERENCES

(1) George, N. C.; Denault, K. A.; Seshadri, R. Phosphors for Solid-State White Lighting. *Annu. Rev. Mater. Res.* **2013**, *43*, 481−501.
(2) Pust, P.; Schmidt, P. J.; Schnick, W. A revolution in lighting. *Nat. Mater.* **2015**, *14*, 454−458.
(3) Wang, L.; Xie, R.-J.; Suehiro, T.; Takeda, T.; Hirosaki, N. Down-Conversion Nitride Materials for Solid State Lighting: Recent Advances and Perspectives. *Chem. Rev.* **2018**, *118*, 1951−2009.
(4) Lougheed, T. Hidden blue hazard? LED lighting and retinal damage in rats. *Environ. Health Perspect.* **2014**, *122*, No. A81.
(5) Daicho, H.; Iwasaki, T.; Enomoto, K.; Sasaki, Y.; Maeno, Y.; Shinomiya, Y.; Aoyagi, S.; Nishibori, E.; Sakata, M.; Sawa, H.; Matsuishi, S.; Hosono, H. A novel phosphor for glareless white light-emitting diodes. *Nat. Commun.* **2012**, *3*, No. 1132.
(6) McKittrick, J.; Hannah, M. E.; Piquette, A.; Han, J. K.; Choi, J. I.; Anc, M.; Galvez, M.; Lugauer, H.; Talbot, J. B.; Mishra, K. C. Phosphor Selection Considerations for Near-UV LED Solid State Lighting. *ECS J. Solid State Sci. Technol.* **2013**, *2*, R3119−R3131.
(7) US Department of Energy *Solid State Lighting Research and Development Plan*. https://www.energy.gov/eere/ssl/downloads/2018-solid-state-lighting-rd-opportunities (accessed 13 March, 2019).
(8) Dai, P.-P.; Li, C.; Zhang, X.-T.; Xu, J.; Chen, X.; Wang, X.-L.; Jia, Y.; Wang, X.; Liu, Y.-C. A single Eu^{2+}-activated high-color-rendering oxychloride white-light phosphor for white-light-emitting diodes. *Light: Sci. Appl.* **2016**, *5*, No. e16024.
(9) Durach, D.; Neudert, L.; Schmidt, P. J.; Oeckler, O.; Schnick, W. $La_3BaSi_5N_9O_2$:Ce^{3+}-A yellow phosphor with an unprecedented tetrahedra network structure investigated by combination of electron microscopy and synchrotron X-ray diffraction. *Chem. Mater.* **2015**, *27*, 4832−4838.
(10) Zhu, Q.-Q.; Wang, L.; Hirosaki, N.; Hao, L. Y.; Xu, X.; Xie, R.-J. Extra-Broad Band Orange-Emitting Ce^{3+}-Doped $Y_3Si_5N_9O$ Phosphor for Solid-State Lighting: Electronic, Crystal Structures and Luminescence Properties. *Chem. Mater.* **2016**, *28*, 4829−4839.
(11) Shang, M.; Li, C.; Lin, J. How to produce white light in a single-phase host? *Chem. Soc. Rev.* **2014**, *43*, 1372−1386.
(12) Gautier, R.; Li, X.; Xia, Z.; Massuyeau, F. Two-Step Design of a Single-Doped White Phosphor with High Color Rendering. *J. Am. Chem. Soc.* **2017**, *139*, 1436−1439.
(13) Marchuk, A.; Schnick, W. $Ba_3P_5N_{10}Br$:Eu^{2+}: a natural-white-light single emitter with a zeolite structure type. *Angew. Chem.* **2015**, *127*, 2413−2417.
(14) Guo, N.; Huang, Y.; You, H.; Yang, M.; Song, Y.; Liu, K.; Zheng, Y. $Ca_9Lu(PO_4)_7$:Eu^{2+},Mn^{2+}: A Potential Single-Phased White-Light-Emitting Phosphor Suitable for White-Light-Emitting Diodes. *Inorg. Chem.* **2010**, *49*, 10907−10913.
(15) Blasse, G.; Grabmaier, B. C. *Luminescent Materials*; Springer: Berlin, Heidelberg, 1994.
(16) Hirosaki, N.; Takeda, T.; Funahashi, S.; Xie, R.-J. Discovery of New Nitridosilicate Phosphors for Solid State Lighting by the Single-Particle-Diagnosis Approach. *Chem. Mater.* **2014**, *26*, 4280−4288.
(17) Liao, H.; Zhao, M.; Molokeev, M. S.; Liu, Q.; Xia, Z. Learning from a Mineral Structure toward an Ultra-Narrow-Band Blue-Emitting Silicate Phosphor $RbNa_3(Li_3SiO_4)_4$:Eu^{2+}. *Angew. Chem.* **2018**, *130*, 11902−11905.
(18) Park, W. B.; Shin, N.; Hong, K.-P.; Pyo, M.; Sohn, K.-S. A New Paradigm for Materials Discovery: Heuristics-Assisted Combinatorial Chemistry Involving Parameterization of Material Novelty. *Adv. Funct. Mater.* **2012**, *22*, 2258−2266.
(19) Correa-Baena, J.-P.; Hippalgaonkar, K.; van Duren, J.; Jaffer, S.; Chandrasekhar, V. R.; Stevanovic, V.; Wadia, C.; Guha, S.; Buonassisi, T. Accelerating Materials Development via Automation, Machine Learning, and High-Performance Computing. *Joule* **2018**, *2*, 1410−1420.
(20) Isayev, O.; Oses, C.; Toher, C.; Gossett, E.; Curtarolo, S.; Tropsha, A. Universal fragment descriptors for predicting properties of inorganic crystals. *Nat. Commun.* **2017**, *8*, No. 15679.
(21) Wang, Z.; Ha, J.; Kim, Y. H.; Im, W. B.; McKittrick, J.; Ong, S. P. Mining Unexplored Chemistries for Phosphors for High-Color-Quality White-Light-Emitting Diodes. *Joule* **2018**, *2*, 914−926.
(22) Zhuo, Y.; Tehrani, A. M.; Oliynyk, A. O.; Duke, A. C.; Brgoch, J. Identifying an efficient, thermally robust inorganic phosphor host via machine learning. *Nat. Commun.* **2018**, *9*, No. 4377.
(23) Kim, M.; Singh, S. P.; Lee, J.-W.; Izawa, T.; Kim, D.; Yun, B.; Yoon, C.; Park, W. B.; Sohn, K.-S. Identification of a narrow band red light-emitting phosphor using computational screening of ICSD: Its synthesis and optical characterization. *J. Alloys Compd.* **2019**, *774*, 338−346.
(24) Park, W. B.; Singh, S. P.; Kim, M.; Sohn, K.-S. Phosphor Informatics Based on Confirmatory Factor Analysis. *ACS Comb. Sci.* **2015**, *17*, 317−325.
(25) Lin, C. C.; Tsai, Y.-T.; Johnston, H. E.; Fang, M.-H.; Yu, F.; Zhou, W.; Whitfield, P.; Li, Y.; Wang, J.; Liu, R.-S. Enhanced Photoluminescence Emission and Thermal Stability from Introduced Cation Disorder in Phosphors. *J. Am. Chem. Soc.* **2017**, *139*, 11766−11770.
(26) Wang, L.; Xie, R.-J.; Li, Y.; Wang, X.; Ma, C.-G.; Luo, D.; Takeda, T.; Tsai, Y.-T.; Liu, R.-S.; Hirosaki, N. $Ca_{1-x}Li_xAl_{1-x}Si_{1+x}N_3$:$Eu^{2+}$ solid solutions as broadband, color-tunable and thermally robust red phosphors for superior color rendition white light-emitting diodes. *Light: Sci. Appl.* **2016**, *5*, No. e16155.
(27) Xie, R.-J.; Hintzen, H. T. Optical Properties of (Oxy)Nitride Materials: A Review. *J. Am. Ceram. Soc.* **2013**, *96*, 665−687.
(28) Wang, Z.; Chu, I.-H.; Zhou, F.; Ong, S. P. Electronic Structure Descriptor for the Discovery of Narrow-Band Red-Emitting Phosphors. *Chem. Mater.* **2016**, *28*, 4024−4031.
(29) Jain, A.; Ong, S. P.; Hautier, G.; Chen, W.; Richards, W. D.; Dacek, S.; Cholia, S.; Gunter, D.; Skinner, D.; Ceder, G.; Persson, K. A. Commentary: The materials project: A materials genome approach to accelerating materials innovation. *APL Mater.* **2013**, *1*, No. 011002.
(30) Sun, W.; Dacek, S. T.; Ong, S. P.; Hautier, G.; Jain, A.; Richards, W. D.; Gamst, A. C.; Persson, K. A.; Ceder, G. The thermodynamic scale of inorganic crystalline metastability. *Sci. Adv.* **2016**, *2*, No. e1600225.
(31) Perdew, J. P.; Burke, K.; Ernzerhof, M. Generalized gradient approximation made simple. *Phys. Rev. Lett.* **1996**, *77*, No. 3865.
(32) Dorenbos, P. Thermal quenching of Eu^{2+} 5d-4f luminance in inorganic compounds. *J. Phys.: Condens. Matter* **2005**, *17*, 8103−8111.

DOI: 10.1021/acs.chemmater.9b02505
Chem. Mater. 2019, 31, 6286−6294

(33) Brgoch, J.; DenBaars, S. P.; Seshadri, R. Proxies from Ab initio calculations for screening efficient Ce^{3+} phosphor hosts. *J. Phys. Chem. C* **2013**, *117*, 17955−17959.
(34) Heyd, J.; Scuseria, G. E.; Ernzerhof, M. Hybrid functions based on a screened Coulomb potential. *J. Chem. Phys.* **2003**, *118*, 8207−8215.
(35) Heyd, J.; Scuseria, G. E.; Ernzerhof, M. Erratum: "Hybrid functions based on a screened Coulomb potential" [J. Chem. Phys. 118, 8207 (2003)]. *J. Chem. Phys.* **2006**, *124*, No. 219906.
(36) Brower, R. W.; Meij, S.; Serruys, P. W. A model of asynchronous left ventricular relaxation predicting the bi-exponential pressure decay. *Cardiovasc. Res.* **1983**, *17*, 482−488.
(37) Sohn, K.-S.; Lee, B.; Xie, R.-J.; Hirosaki, N. Rate-equation model for energy transfer between activators at different crystallographic sites in $Sr_2Si_5N_8:Eu^{2+}$. *Opt. Lett.* **2009**, *34*, No. 3427.
(38) Wang, T.; Zheng, P.; Liu, X.; Chen, H.; Yang, S.; Liu, Q. L. Decay Behavior Analysis of Two-Peak Emission in $Ca(Al/Si)_2N_2(N_{1-x}O_x):Eu^{2+}$ Phosphors. *J. Electrochem. Soc.* **2014**, *161*, H25−H28.
(39) Lu, F.-C.; Bai, L.-J.; Dang, W.; Yang, Z.-P.; Lin, P. Structure and Photoluminescence of Eu^{2+} Doped $Sr_2Al_2SiO_7$ Cyan-Green Emitting Phosphors. *ECS J. Solid State Sci. Technol.* **2015**, *4*, R27−R30.
(40) Li, Y. Q.; Hirosaki, N.; Xie, R.-J.; Mitomo, M. Crystal, electronic and luminescence properties of Eu^{2+}-doped $Sr_2Al_{2-x}Si_{1+x}O_{7-x}N_x$. *Sci. Technol. Adv. Mater.* **2007**, *8*, 607−616.
(41) Li, G.; Tian, Y.; Zhao, Y.; Lin, J. Recent progress in luminescence tuning of Ce^{3+} and Eu^{2+}-activated phosphors for pc-WLEDs. *Chem. Soc. Rev.* **2015**, *44*, 8688−8713.
(42) Wang, Z.; Ye, W.; Chu, I.-H.; Ong, S. P. Elucidating Structure-Composition-Property Relationships of the β-SiAlON:Eu^{2+} Phosphor. *Chem. Mater.* **2016**, *28*, 8622−8630.
(43) Tu, B.; Liu, X.; Wang, H.; Wang, W.; Zhai, P.; Fu, Z. Combining 27Al Solid-State NMR and First-Principles Simulations To Explore Crystal Structure in Disordered Aluminum Oxynitride. *Inorg. Chem.* **2016**, *55*, 12930−12937.
(44) Xia, Z.; Ma, C.; Molokeev, M. S.; Liu, Q.; Rickert, K.; Poeppelmeier, K. R. Chemical Unit Cosubstitution and Tuning of Photoluminescence in the $Ca_2(Al_{1-x}Mg_x)(Al_{1-x}Si_{1+x})O_7:Eu^{2+}$ Phosphor. *J. Am. Chem. Soc.* **2015**, *137*, 12494−12497.
(45) Koroglu, A.; Thompson, D. P.; Apperley, D. C.; Harris, R. K. Oxygen/nitrogen ordering in lanthanum new phase ($La_3Si_8N_{11}O_4$). *J. Solid State Chem.* **2004**, *177*, 2530−2533.
(46) Pust, P.; Weiler, V.; Hecht, C.; Tücks, A.; Wochnik, A. S.; Henß, A. K.; Wiechert, D.; Scheu, C.; Schmidt, P. J.; Schnick, W. Narrow-band red-emitting $Sr[LiAl_3N_4]:Eu^{2+}$ as a next-generation LED-phosphor material. *Nat. Mater.* **2014**, *13*, 891−896.
(47) Kresse, G.; Furthmüller, J. Efficient iterative schemes for ab initio total-energy calculations using a plane-wave basis set. *Phys. Rev. B* **1996**, *54*, No. 11169.
(48) Blöchl, P. E. Projector augmented-wave method. *Phys. Rev. B* **1994**, *50*, No. 17953.
(49) Ong, S. P.; Richards, W. D.; Jain, A.; Hautier, G.; Kocher, M.; Cholia, S.; Gunter, D.; Chevrier, V. L.; Persson, K. A.; Ceder, G. Python Materials Genomics (pymatgen): A robust, open-source python library for materials analysis. *Comput. Mater. Sci.* **2013**, *68*, 314−319.
(50) Togo, A.; Tanaka, I. First principles phonon calculations in materials science. *Scr. Mater.* **2015**, *108*, 1−5.
(51) Giannozzi, P.; Andreussi, O.; Brumme, T.; Bunau, O.; Nardelli, M. B.; Calandra, M.; Car, R.; Cavazzoni, C.; Ceresoli, D.; Cococcioni, M.; et al. Advanced capabilities for materials modelling with Quantum ESPRESSO. *J. Phys.: Condens. Matter* **2017**, *29*, No. 465901.
(52) Perdew, J. P.; Zunger, A. Self-interaction correction to density-functional approximations for many-electron systems. *Phys. Rev. B* **1981**, *23*, No. 5048.
(53) Dudarev, S. L.; Botton, G. A.; Savrasov, S. Y.; Humphreys, C. J.; Sutton, A. P. Electron-energy-loss spectra and the structural stability of nickel oxide: An LSDA+U study. *Phys. Rev. B* **1998**, *57*, No. 1505.
(54) Chaudhry, A.; Boutchko, R.; Chourou, S.; Zhang, G.; Grønbech-Jensen, N.; Canning, A. First-principles study of luminescence in Eu^{2+}-doped inorganic scintillators. *Phys. Rev. B* **2014**, *89*, No. 155105.
(55) Hautier, G.; Fischer, C.; Ehrlacher, V.; Jain, A.; Ceder, G. Data mined ionic substitutions for the discovery of new compounds. *Inorg. Chem.* **2011**, *50*, 656−663.
(56) Bergerhoff, G.; Hundt, R.; Sievers, R.; Brown, I. D. The inorganic crystal structure data base. *J. Chem. Inf. Model.* **1983**, *23*, 66−69.
(57) Toby, B. H. EXPGUI, a graphical user interface for GSAS. *J. Appl. Crystallogr.* **2001**, *34*, 210−213.

DOI: 10.1021/acs.chemmater.9b02505
Chem. Mater. 2019, 31, 6286−6294